Effect of Titanium on Copper-Titanium / Carbon Nanofibre Composite Materials

J.C. Lloyd, E. Neubauer, J. Barcena, W.J. Clegg

Accepted Manuscript

Effect of Titanium on Copper-Titanium / Carbon Nanofibre Composite Materials

J.C. Lloyd, E. Neubauer, J. Barcena, W.J. Clegg

PII: S0266-3538(10)00174-0
DOI: 10.1016/j.compscitech.2010.05.002
Reference: CSTE 4705

To appear in: *Composites Science and Technology*

Received Date: 17 November 2009
Revised Date: 13 April 2010
Accepted Date: 3 May 2010

Please cite this article as: Lloyd, J.C., Neubauer, E., Barcena, J., Clegg, W.J., Effect of Titanium on Copper-Titanium / Carbon Nanofibre Composite Materials, *Composites Science and Technology* (2010), doi: 10.1016/j.compscitech.2010.05.002

Effect of Titanium on Copper-Titanium / Carbon Nanofibre Composite Materials

J. C. Lloyd[a], E. Neubauer[b], J. Barcena[c] and W. J. Clegg[a*]

[a]Gordon Laboratory, Department of Materials Science and Metallurgy, University of Cambridge, Pembroke Street, Cambridge CB2 3QZ, United Kingdom.

[b]Austrian Institute of Technology, 2444 Seibersdorf, Austria.

[c]INASMET Tecnalia, Mikeletegi Pasealekua, 2 Parque Tecnológico / Teknologi Parkea E-20009 Donostia - San Sebastian.

*Corresponding author. Tel.: +44 1223334470; Fax.:+44 1223334567; E-mail address: wjc1000@cam.ac.uk

Abstract

Copper/carbon nanofibre composites containing titanium varying from 0.3wt% to 5wt% were made, and their thermal conductivities measured using the laser flash technique. The measured thermal conductivities were much lower than predicted. The difference between measured and predicted values has often been attributed to limited heat flow across the interface. A study has been made of the composite microstructure using x-ray diffraction, transmission electron microscopy and Raman spectroscopy. It is shown in these materials, that the low composite thermal conductivity arises primarily because the highly graphitic carbon nanofibre structure transforming to amorphous carbon during the fabrication process.

Keywords: A. Metal-matrix composite (MMCs); A. Carbon Nanofibre; B. Thermal properties; D. Raman Spectroscopy, D. Transmission Electron Microscopy (TEM)

1. Introduction

Effective thermal management in modern power electronics requires a heat sink material with as high a thermal conductivity as possible [1]. Carbon based materials such as diamond and carbon nanofibres exhibit high thermal conductivity values, 1500 – 2000 [2] and 1200 W m^{-1} K^{-1} [3], respectively.

High thermal conductivity composites, for example synthetic Ib-type diamond inclusions embedded in a silver-11at%silicon matrix, have been fabricated exhibiting high thermal conductivity values of 970 W m^{-1} K^{-1} at an inclusion volume fraction of 0.76 [4]. Unfortunately, these composites are difficult to machine due to the high hardness of diamond [5]. Therefore, composites containing carbon nanofibre inclusions potentially combine high thermal conductivities with the ease of machinability.

In studies of metal matrix composites containing carbon-based inclusions, the main area of concern has been the quality of interfacial bonding between the metal matrix and carbon inclusion [5, 6]. This is because inert metals, such as copper and silver, do not wet carbon and no physical bond is formed at the interface [6]. Wetting has been enhanced by alloying with carbide forming additives, such as chromium and titanium, which diffuse to the carbon surface and react to form a thin, continuous carbide interlayer [7].

In this work, copper/carbon nanofibre composites were fabricated using a powder metallurgical route where titanium was added to enhance interfacial bonding. The aim of this work was to study the effect of varying the

concentration of titanium and to correlate the microstructure of these composites with the measured thermal conductivities.

2. Experimental Techniques

2.1 Composite Fabrication

The composites were fabricated using a powder metallurgy technique [8], which involves coating Showa Denko carbon nanofibres [3] with copper, using an electroless deposition technique. Different chemical solutions are used to sensitise (SnCl) and activate (PdCl) the surface of the carbon nanofibres, before plating with copper [9]. The amount of copper deposited yielded composites with a fibre volume fraction of 0.2, assuming a fibre density of 2.0 g cm^{-3}. After the copper deposition process, the copper coated carbon nanofibres was washed and dried. Following this, titanium powder (50 nm and 45 μm, contains 0.05 – 0.4 wt% oxygen) was admixed and the final powder mixture was hot pressed in a graphite die at 900 - 1000 ^{o}C under a pressure of 35 MPa. This results in a composite with a 2-D random fibre arrangement. Further details of the composite fabrication process can be found in [8]. The composites were identified using the following notation CuTi(Xwt%)/CNF where X denotes the amount of titanium introduced to the system.

2.2 Thermal Measurements

The room temperature thermal diffusivity, *D*, of these composites were measured in the transverse direction, parallel to the hot-pressing direction, using a transient thermal flash technique (Netzsch LFA 457 Microflash^{TM}). Measurements were made on cylindrical discs 6 mm in diameter and 4 mm

thick. Composite thermal conductivity, κ, was determined from measurements of composite density, ρ, and specific heat capacity, C, using the relationship [10] $\kappa = D\rho C$. Specific heat capacity was measured using differential scanning calorimetry (TA-Instruments Q100) on cylindrical discs 4 mm in diameter and 0.5 mm thick. Composite density was determined using the Archimedes technique, using perfluoromethyldecalin (Flutec PP9, ρ = 1.96 g cm^{-3}) as the fluid medium.

2.3 Characterisation of Composite

2.3.1 Phase-identification

The phases in the composite were determined using X-ray diffraction. Standard θ – 2θ traces were recorded on a diffractometer (Phillips PW1820) from 20 – 90^{o}, using a Cu Kα radiation source operated at 40kV accelerating voltage and 40 mA filament current. The beam was narrowed using 1/2^{o} divergence and anti-scatter slits, and a 0.2 mm receiving slit. The signal was recorded at a step size of 0.025^{o} and a dwell time of 12.5 s. Phase identification was carried out on the Xpert Highscore Plus programme and quantification was achieved by Rietveld analysis.

2.3.1 Microstructural Characterisation

The overall composite microstructure was observed in the dual beam FIB (Helios Nanolab SEM/FIB), where focused ion beam (FIB) milling was used to prepare the sample surface for viewing in the scanning electron microscope (SEM).

Teansmission electron microscopy (TEM) samples were prepared using the trench technique in the FIB (FEI 200 FIB workstation) and studied in the

transmission electron microscopes (CM30 and Tecnai FEI20), using acceleration voltages of 300 and 200 keV, respectively. Elemental analysis was performed, where elemental mapping of titanium, copper and carbon was carried out using energy filtered TEM (EFTEM). The K– and L–edges of copper and titanium from electron energy loss spectroscopy (EELS) was used to determine the bonding nature of these elements. EELS spectra were acquired at 1 nm intervals along the line of interest. Quantitative analysis was then carried out using the ES Vision FEI software.

Raman spectroscopy was used to determine the level of graphitization in the carbon nanofibre, using a micro-Raman system (Ramascope-1000) with a 633 nm red laser monochromator source. All spectra were collected through a 50× objective lens, whereby the laser spot size was approximately 10 μm in diameter. The Raman spectra exhibits three characteristic peaks: the D-peak arising from defects and disorder, for example grain boundaries, broken sp^2 C bonds and sp^3 C); the G-peak is a result of the graphitic structure within the sample; and the G′ peak is due to long range order [11, 12]. Relative changes in defect concentration was monitored using the D/G peak ratio, where a small ratio corresponds to an ordered and highly crystalline material.

3. Results and Discussion

3.1 Composite Thermal Conductivity

The thermal conductivity of the Cu/CNF composite, in the transverse direction, was 255 ± 35 W m^{-1} K^{-1}. Figure 1 shows the variation in composite thermal conductivity, in the transverse direction, with titanium concentration.

The introduction of 0.3 wt% titanium (50 nm) resulted in a 22% increase in composite thermal conductivity (311 W m^{-1} K^{-1}). Further additions of titanium to the copper coated carbon nanofibres reduced the composite thermal conductivity. At 5 wt% titanium (200 W m^{-1} K^{-1}), a reduction of 35% from peak value was observed. These low composite values are comparable to other previously studied copper-alloy/CNF composites, where the resultant composite thermal conductivity lies below that of copper [13, 14], which is expected in randomly arranged fibre composites containing highly anisotropic fibres [15].

Predictions were made for a 0.2 volume fraction 2-D randomly aligned fibre composite, using the relationships in [15], assuming perfect thermal conduction at the interface (infinite interface thermal conductance), a matrix thermal conductivity of κ_m = 400 W m^{-1} K^{-1} and various fibre properties. For a composite containing isotropic fibres, κ_f = 1200 W $m^{-1}K^{-1}$, the composite was expected to have a thermal conductivity of 526 W $m^{-1}K^{-1}$ (in-plane) and 489 W $m^{-1}K^{-1}$ (transverse). Most carbon fibres are anisotropic, taking an anisotropy ratio comparable to K1100 carbon fibre (Cytec [16]), κ_f^{long} = 1200 W m^{-1} K^{-1} and κ_f^{trans} = 3 W $m^{-1}K^{-1}$, the composite thermal conductivity was estimated to be 401 W m^{-1} K^{-1} (in-plane) and 268 W m^{-1} K^{-1} (transverse). When κ_f = 0 W m^{-1} K^{-1} there was no difference in the transverse direction properties (267 W m^{-1} K^{-1}). The Cu/CNF and CuTi(Xwt%)/CNF composite thermal conductivities (200 - 311 W m^{-1} K^{-1}) are very similar to predictions where the fibres are have low transverse thermal conductivity.

Taking into consideration poor transverse fibre properties (a few W m-1 K^{-1}) the variations in composite thermal conductivity with titanium content arises

from changes in matrix properties, as it is known that alloying reduces the thermal conductivity of copper. Figure 2 shows the thermal conductivity of copper rapidly reduced from 400 $Wm^{-1}K^{-1}$ to 175 $Wm^{-1}K^{-1}$ after alloying with 1 wt% titanium [17]. It is observed that the composite thermal conductivity does not fall as drastically with titanium content as that of copper. This is a due to the removal of titanium from the matrix as a result of titanium carbide formation. At high addition of titanium powders, the remains of titanium particles could still be observed, which reduces the effective matrix thermal conductivity and thus the composite thermal conductivity.

3.2 Study of Composite Microstructure

Results presented are primarily on the CuTi(5wt%)/CNF material, where there is an ease in identifying phases and at reasonable quantities. The CuTi(5wt%)/CNF composite microstructure is very inhomogeneous, Figure 3, consisting of both well-dispersed and agglomerated carbon nanofibres, titanium agglomerates and voids. In regions with a high titanium content, see top right of micrograph, the carbon nanofibres are coated with a titanium carbide interlayer. Carbon nanofibres at a distance greater than the diffusion distance of titanium in copper under the consolidation conditions, 35 μm, from any titanium powder will not have this interlayer, as shown by the carbon nanofibre agglomerate at the bottom left corner of the micrograph. It should be noted that a more homogeneous structure was observed in the CuTi(0.3wt%)/CNF composite.

3.2.1 Phase-Identification

From the X-ray diffraction profile, Figure 4, the main phase in the composite was copper. The observed trace also confirmed the presence of Cu_2O (2 wt%), TiC (5 wt%) and β-CuPd (2 wt%). Oxygen analysis of the composites complements the XRD analysis, as the average oxygen content was 0.35 wt% [8]. Both the Cu_2O and β-CuPd are impurities arising from the composite fabrication process. Measurements on other composite samples show that β-CuPd was not uniformly distributed throughout the composite material, as it was only observed in 10% of the samples.

Elemental mapping of carbon, copper and titanium using EFTEM, Figure 5, confirms the diffusion of titanium to the copper/carbon nanofibre interface to form titanium carbide. The titanium carbide layer is approximately 80 to 140 nm thick. This is quite a severe reaction, as a majority of the fibres have a diameter of 150 nm and would be totally converted into titanium carbide. The intrinsic thermal conductivity of titanium carbide is approximately 30 $Wm^{-1}K^{-1}$ [18, 19]. Therefore thick layers of titanium carbide are undesirable, as they act as a physical thermal barrier to heat flow across the interface. The extent of titanium carbide formation can be limited by reducing the amount of titanium.

From the near edge structure of EELS spectra, the bonding nature of the elements was probed, where in Figure 6b and 6c the carbon K-edge corresponds to a mixture of sp^2 and sp^3 bonded carbon, and carbon bonded to titanium, respectively. The collection of EELS spectra at the titanium carbide/carbon interface, Figure 6a, was quantitatively analysed giving titanium to carbon ratio of 0.94 to 1 in the titanium carbide layer.

Further study of the EELS spectra, Figure 6d, revealed that titanium diffused 14 nm ahead of the titanium carbide/carbon nanofibre interface without bonding to carbon. Titanium was first detected at 27 nm, whilst titanium carbide was only observed at 40 nm. The titanium content in the carbide layer increases to a constant ratio over a distance of 47 nm.

3.2.2 Carbon Nanofibre Structure

In the TEM, the surface of the carbon nanofibre in contact with the titanium carbide layer was observed to be amorphous, Figure 7. This was determined using electron diffraction. Two patterns were recorded, one at the centre of the carbon nanofibre (position Y), Figure 7b, and the other close to the carbide interface layer (position X), Figure 7c. The electron diffraction pattern at the centre of the carbon nanofibre, indicates that there is long range order, as sharp (002) diffraction spots are observed. Amorphous halo rings are observed in Figure 7c. In the fibre studied, the amorphous carbon layer is approximately 430 nm thick, where two-thirds of the fibre is no longer graphitic.

The high thermal conductivity of carbon fibres arise from their highly graphitic structure [20]. Therefore, the transformation of graphitic carbon to amorphous carbon results in a reduction in the thermal conductivity. A qualitative study of the variations in graphite content between the fabricated composites was carried out using Raman spectroscopy by studying the D/G peak ratio. The measured values have been summarized in Table 1.

The D/G peak ratio for the as-received fibre was very low at 0.12. Upon consolidation in the composite without any additive material, the D/G peak ratio

increased to 0.97. Composites with titanium exhibit similarly high D/G peak ratios. The Raman results confirm observation in the TEM, that the carbon fibres have lost their highly crystalline structure.

4. Conclusions

Raman spectra from the carbon nanofibre material in the composites show a loss of fibre crystallinity, where graphitic carbon undergoes an amorphous transformation. This crystalline to amorphous transformation reduces the effective thermal conductivity of the carbon nanofibres and thus accounts for the low composite thermal conductivities observed. Observations of the composite microstructure reveal that the titanium additives diffuse to the carbon nanofibre surface and reacts to form titanium carbide, $Ti_{0.94}C$. In the case of high titanium contents, the reaction is severe where whole carbon nanofibres are converted into titanium carbide, which corresponds to the Raman D/G peak ratios. The presence of titanium particles in the copper matrix, as well as other impurity phases, such as copper oxide and copper palladium, reduces the effective thermal conductivity of the matrix, further diminishing the composite thermal conductivity.

In order to achieve high thermal conductivity composites from these materials, the graphitic nature of the carbon nanofibres needs to be preserved. Further work, would be to determine when in the fabrication process and how this transformation takes place. It is suggested that this occurs by:

1. Interaction between titanium atoms which have diffused into carbon vacancy sites. The formation of the Ti-C bond disrupts the ordered

graphitic structure, as the Ti-C bond lengths (2.17 Å) is dissimilar to the C-C bond (1.42 Å) and graphite interplanar (3.394 Å) distance.

2. The carbon nanofibre material acts as a reducing agent for copper and titanium oxides during the hot-pressing process, consuming the carbon nanofibre.

Acknowledgements

This work was supported by the FP6 EU project STRP 031712 INTERFACE and AGAPAC Project, REF: 218851 / FP7-SPACE-CALL-1. The authors would like to thank Dr Mary Vickers, Dr Richard Beanland and Dr Jonathan Barnard for their assistance in this work.

References

[1] C. Zweben. Thermal materials solve power electronics challenges. Power Electronics Technology, 32(2):40–47, 2006.

[2] R. Tavangar, J. M. Molina, and L. Weber. Assessing predictive schemes for thermal conductivity against diamond-reinforced silver matrix composites at intermediate phase contrast. Scripta Materialia, 56(5):357–360, 2007.

[3] Showa Denko Carbon Inc. Vapour grown carbon fibre (VGCF-H) http://www.sdkc.com/documents/VGCF-H.pdf (Viewed July 2009).

[4] L. Weber and R. Tavangar. Diamond-based metal matrix composites for thermal management: Potential and limits. Advanced Materials Research, 59:111-115, 2009

[5] F. A. Khalid, O. Beffort, U. E. Klotz, B. A. Keller, and P. Gasser. Microstructure and interfacial characteristics of aluminium-diamond composite materials. Diamond and Related Materials, 13(3):393–400, 2004.

[6] T. Schubert, L. Ciupinski, W. Zielinski, A. Michalski, T. Weissgaeber, and B. Kieback. Interfacial characterization of Cu/diamond composites prepared by powder metallurgy for heat sink applications. Scripta Materialia, 58(4):263–266, 2008.

[7] D. A. Mortimer and M. Nicholas. The wetting of carbon by copper and copper alloys. Journal of Materials Science, 5:149 – 155, 1970.

[8] J. Barcena, J. Maudes, J. Coleto, J. L. Baldonedo, and J. M. Gomez de Salazar. Microstructural study of vapour grown carbon nanofibre/copper composites. Composites Science and Technology, 68(6):1384 – 1391, 2008.

[9] L. M. Ang, T. S. A. Hor, G. Q. Xu, C. H. Tung, S. P. Zhao, and J. L. S. Wang. Decoration of activated carbon nanotubes with copper and nickel. Carbon, 38(3):363 – 372, 2000.

[10] A. Salazar. On thermal diffusivity. European Journal of Physics, 24(4):351–358, 2003.

[11] F. Tuinstra and J. L. Koenig. Raman spectrum of graphite. The Journal of Chemical Physics, 53(3):1126–1130, 1970.

[12] R. A. DiLeo, B. J. Landi, and R. P. Raffaelle. Purity assessment of multiwalled carbon nanotubes by Raman spectroscopy. Journal of Applied Physics, 101(6), 2007.

[13] C. Edtmaier, T. Janhsen, R. C. Hula, L. Pambaguian, H. G. Wulz, S. Forero, and F. Hepp. Carbon Nanotubes as Highly Conductive Nano-Fillers in Metallic Matrices. In C. Linsmeier and M. Reinelt, editors, 1st International Conference on New Materials for Extreme Environments, volume 59 of Advanced Materials Research, pages 131–137, 2009.

[14] E. Neubauer, M. Kizmantel, C. Eisenmenger-Sittner, I. Smid, and P. Angerer. Copper based composites reinforced with carbon nanofibres. Advances in Powder Metallurgy and Particulate Materials, 2:1 – 9, 2007.

[15] J. C. Lloyd and W. J. Clegg. Effect of Fibre Anisotropy on Composite Thermal Conductivity. Advanced Materials Research 59:148–152, 2009

[16] Cytec Industries. Thornel K-1100 Continuous Pitch-Based Fibre, Viewed in August 2009. http://www.cytec.com/engineered-materials/products/cfThornelK-1100pitch.htm.

[17] E. Neubauer. Interface optimisation in copper-carbon metal matrix composites. PhD thesis. Austria: Austrian Institute of Technology, 2003.

[18] L. G. Radosevich and W. S. Williams. Thermal conductivity of transition metal carbides. Journal of the American Ceramic Society, 53:30 – 33, 1970.

[19] W. S. Williams. Physics of transition metal carbides. Materials Science and Engineering A, 105/106:1 – 10, 1988.

[20] L. Piraux, B. Nysten, A. Haquenne, J. P. Issi, M. Dresselhaus, and M. Endo. The temperature variation of the thermal conductivity of benzene-derived carbon fibres. Solid State Communications, 50(8):697 – 700, 1984.

Figure captions

Figure 1: Measured composite thermal conductivity values plotted against titanium additive content. Black circles denote composites made with 50 nm titanium powders whilst blue triangles are for 45 μm powders.

Figure 2: Thermal conductivity of copper falls with titanium additive content. Adapted from [17].

Figure 3: Overall microstructure of CuTi(5wt%)/CNF composite material observed in the SEM. The vertical lines observed is known as curtaining, which is an artifact from FIB milling.

Figure 4: X-ray diffraction pattern from CuTi(5wt%)/CNF composite. Phases were identified as *copper (91 wt%), $^{\xi}$copper oxide (2 wt%), $^{\gamma}$titanium carbide (5 wt%), $^{\Phi}$copper palladium (2 wt%), and $^{\alpha}$carbon.

Figure 5: Elemental maps obtained using energy filtered transmission electron microscopy of (a) carbon; (b) copper and (c) titanium from the CuTi(5wt%)/CNF composite.

Figure 6: Quantitative elemental analysis at the titanium carbide/carbon nanofibre interface using electron energy loss spectroscopy (EELS), where (a) the scanning transmission electron micrograph, showing the line in which EELS spectra was collected; (b) the EELS spectra from position Y, where the C-K and Ti-L edges are observed; (c) the EELS spectra of carbon; and (c) plot of normalized carbon and titanium content with distance.

Figure 7: TEM micrograph of CuTi(5wt%)/CNF composite, showing (a) a single CNF embedded in the copper matrix; (b) diffraction pattern from the centre of the fibre, position Y, exhibiting sharp (002) diffraction spots; and (c) diffraction pattern from the surface of the fibre, position X, consisting of diffuse halo rings from amorphous carbon.

Table 1 Raman spectra D/G peak ratio from as received carbon nanofibre and composite materials.

Material	D/G peak ratio
Carbon nanofibre	0.12 ± 0.05
Cu/CNF composite	0.97 ± 0.30
CuTi(0.3wt%)/CNF composite	1.23 ± 0.31
CuTi(0.5wt%)/CNF composite	1.36 ± 0.29
CuTi(1.5wt%)/CNF composite	1.06 ± 0.31
CuTi(5wt%)/CNF composite	0.95 ± 0.28

Figure 1

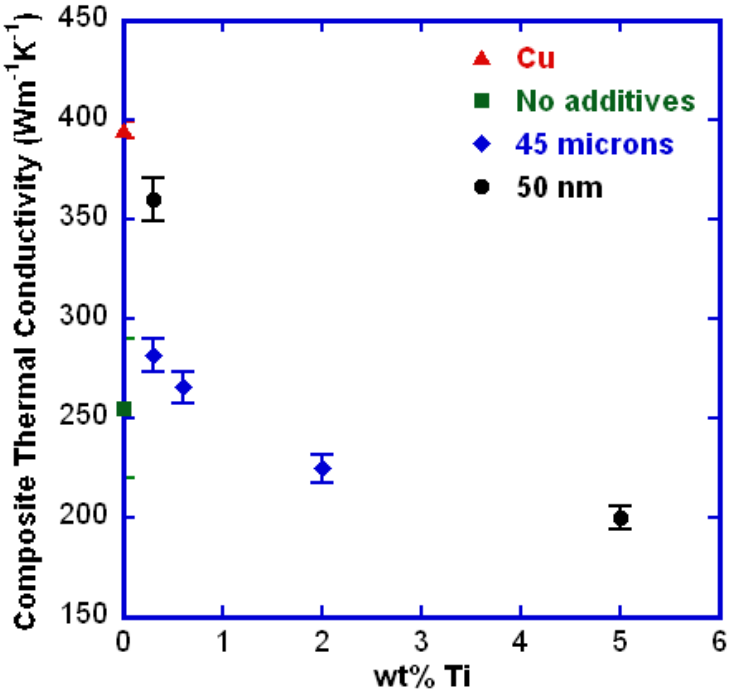

Figure 2

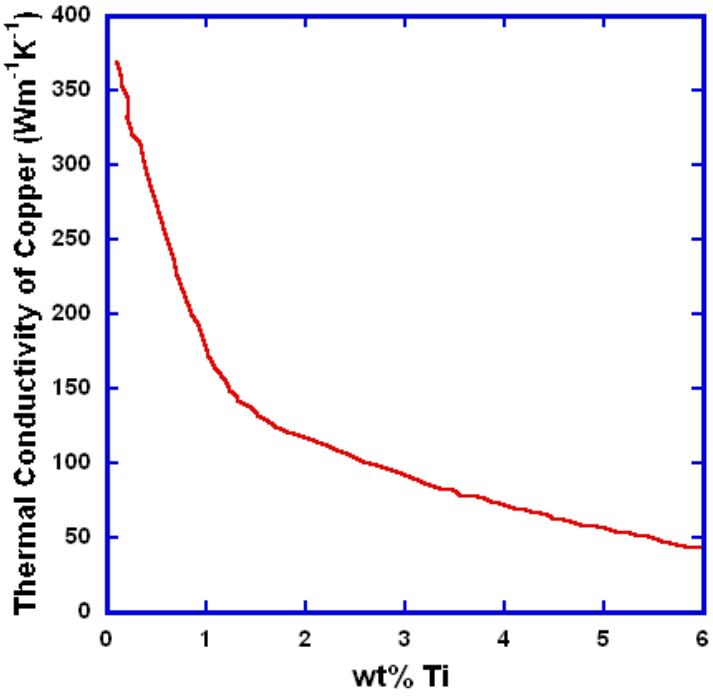

Figure 3

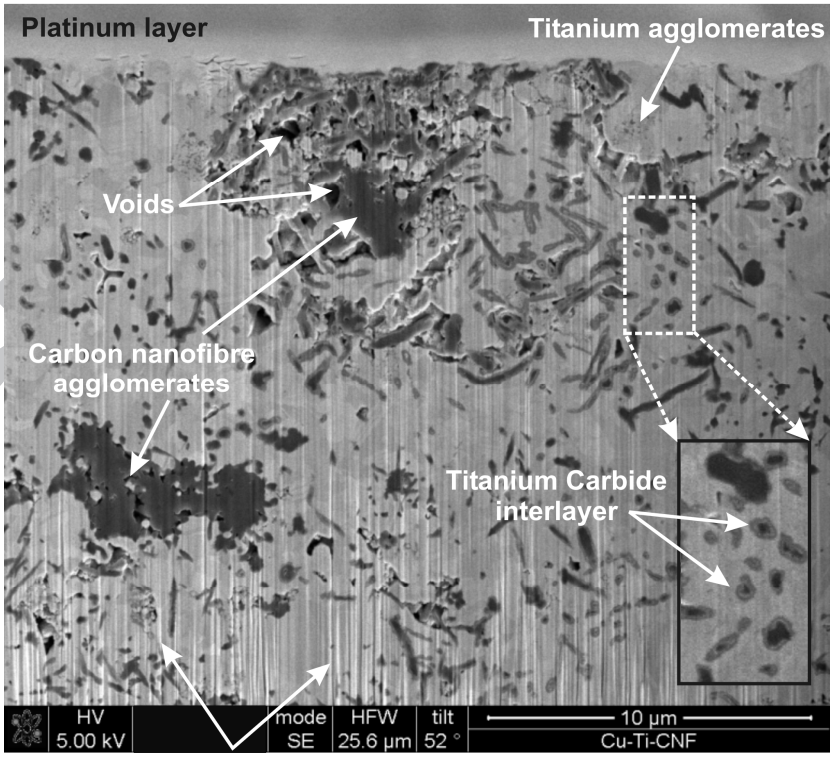

Curtaining from FIB milling

Figure 4

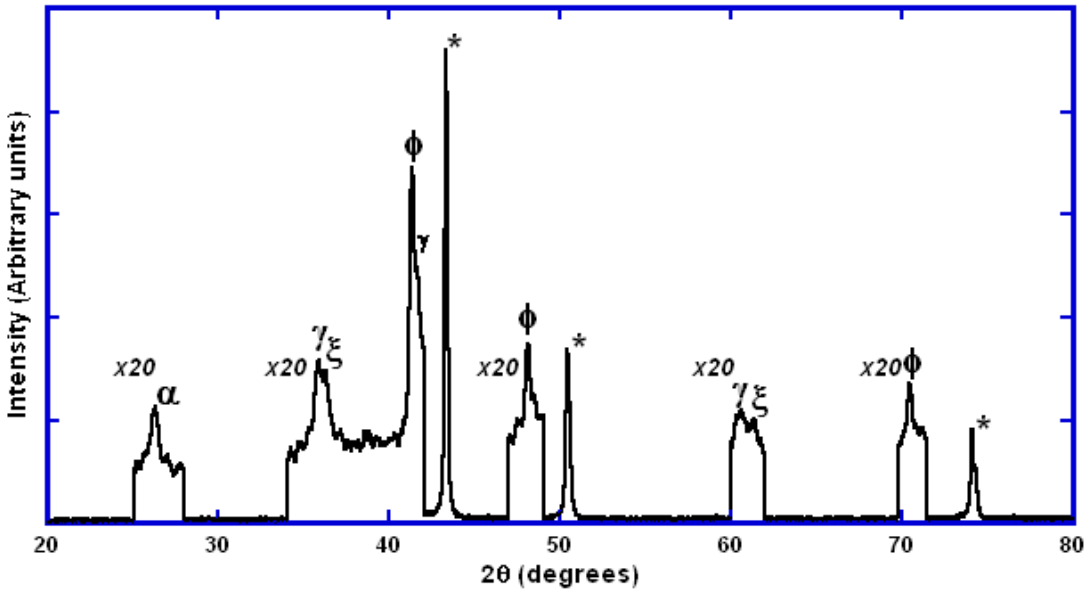

Figure 5

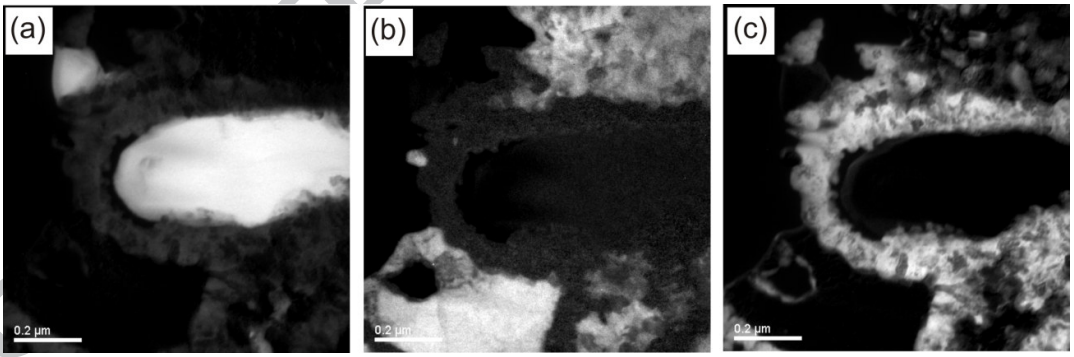

Figure 6

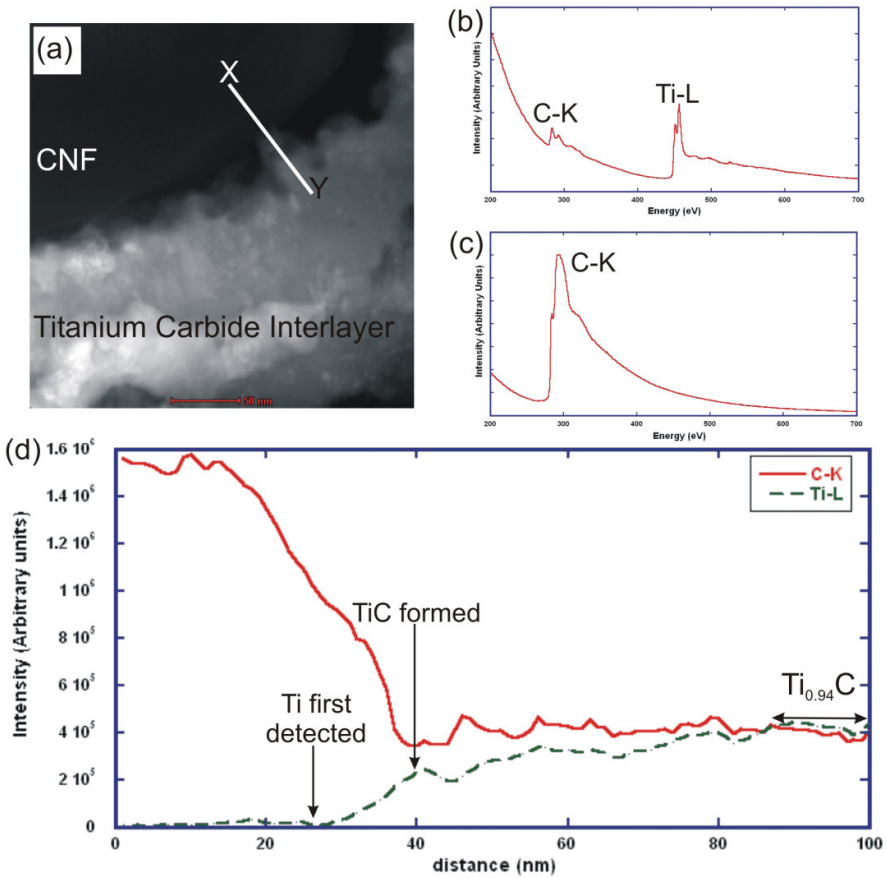

Figure 7